Available online at www.sciencedirect.com
SCIENCE DIRECT®
Journal of Computational Physics 209 (2005) 354–370
JOURNAL OF COMPUTATIONAL PHYSICS
www.elsevier.com/locate/jcp

Modelling of heat transport in magnetised plasmas using non-aligned coordinates

S. Günter [a,*], Q. Yu [a], J. Krüger [b], K. Lackner [a]

[a] Max-Planck Institut für Plasmaphysik, Euratom-Association, 85748 Garching, Germany
[b] Technische Universität München, ZWE FRM-II, 85747 Garching, Germany

Received 5 October 2004; received in revised form 24 February 2005; accepted 7 March 2005
Available online 24 May 2005

Abstract

We present discretisation schemes for the heat diffusion equation in strongly magnetised plasmas in 2-d Cartesian and 3-d cylindrical geometry. The algorithms described do not use field-aligned coordinates, but show, nevertheless, a strong reduction of the pollution of perpendicular heat flux caused by parallel heat conduction, compared to standard finite element or other finite difference formulations. Results for test examples show independence of the numerical error from $\chi_{\|}$ for values of $\chi_{\|}/\chi_{\perp}$ up to 10^9 in plane and 10^{12} in periodic cylinder geometry (simulating toroidal connection). The algorithms appear particularly well suited for dynamic MHD calculations, where the effort of using exactly aligned coordinates becomes prohibitive.

1. Introduction

The strong anisotropy of the heat conductivity in magnetised, high temperature plasmas poses a challenging computational problem. For ratios of the heat conductivity coefficients $\chi_{\|}/\chi_{\perp}$ which can exceed 10^{10} in state of art fusion experiments, pollution by numerical errors can easily swamp the true perpendicular transport. An effective remedy consists in the choice of a coordinate system in which one of the coordinates is aligned with the magnetic field direction. While this is practicable and efficient for the case of given, stationary fields [1–4] or small magnetic perturbations superposed on closed flux surface structures [5], a scheme compatible with a time-independent coordinate system is desirable for dynamic, strongly nonlinear MHD calculations [6–11]. The need for a highly accurate scheme is particularly apparent for the simulation of neoclassical tearing modes [12,13], where the onset requirements for this non-linear instability are largely determined by the balance between parallel and perpendicular heat transport [14].

* Corresponding author. Tel.: +49 89 3299 1718; fax: +49 89 3299 2580.
E-mail address: guenter@ipp.mpg.de (S. Günter).

0021-9991/$ - see front matter © 2005 Elsevier Inc. All rights reserved.
doi:10.1016/j.jcp.2005.03.021

The scheme described in this paper remains – in practically relevant cases – only second-order accurate, but reduces the pollution of perpendicular by parallel transport dramatically. In fact, for the widely used analytical test case [9] the numerical error was found to be independent of the ratio $\chi_\parallel/\chi_\perp$ up to the (unrealistic) tested limit of 10^{12}. We describe the scheme and present tests for two geometries and cases: the steady state solution in a 2-d Cartesian grid (which can be readily extended to 3-d – by either applying the same algorithm also in the 3rd direction, or by adding a Fourier expansion – and to the time-dependent case) and the time dependent problem in a 3-d case in cylinder coordinates, based on a Fourier expansion of the magnetic field and the dependent variables in the azimuthal and axial directions. In both cases we compare the schemes with alternative finite difference or finite element approximations. To explore the range of applicability of the scheme, we have conducted also test-calculations with non-orthogonal coordinates, non-equidistant grids, spatially varying heat conductivity and magnetic fields with non-divergence free $\vec{b} = \vec{B}/|B|$.

Our developments originally started with the recognition that the most straightforward, second order accurate scheme, in the 1-d finite-difference, 2-d Fourier-decomposition case, involved the variable values in different grid points for the representation of temperature gradients in the time advance for the different Fourier components. Defining all components of the parallel temperature gradient in the same points on a staggered grid with respect to the temperatures dramatically improved the convergence behaviour for large values of $\chi_\parallel/\chi_\perp$ and the agreement with known analytic test cases. The extension to the 2-d difference case was an attempt to explore the consequences of the same principle in a multi-dimensional finite grid formulation. Our reference schemes in this case were on one hand a difference formulation extending the usual scheme for an isotropic case by terms describing the anisotropy, and on the other the different order finite element approaches studied by the NIMROD team. Reproducing the test runs described in [9] we were thereby able to see that our scheme not only performed much better than the bi-linear basis-function scheme involving the same grid-variable, but – for high values of $\chi_\parallel/\chi_\perp$ – compared even favourably with the much more involved bi-quadratic and bi-cubic schemes. Our symmetric difference formulation is conservative and maintains also the property of self-adjointness of the differential heat conduction operator [15].

As we have carried out the basic analyses primarily for the time-independent 2-d case, the more practical applications, however, in the 3-d, time-dependent formulation, we present the two schemes in this sequence in the next two chapters. For transparency we relegate the description of the full algorithm for the 3-d case to the appendix.

2. Finite difference formulation in a 2-d Cartesian grid

As we concentrate here on the problems arising from the strong anisotropy of the heat conductivity, we write the temperature evolution equation in a magnetised plasma in the form

$$\frac{3}{2} n \frac{\partial}{\partial t} T = -\nabla \cdot \vec{q} + Q \tag{1}$$

neglecting terms arising from convection and compression heating. As we concentrate on the difficulties arising from the term

$$\vec{q} = -n[\chi_\parallel \vec{b}\vec{b} + \chi_\perp (\overleftrightarrow{I} - \vec{b}\vec{b})] \cdot \nabla T \tag{2}$$

($\vec{b}$ being the unit vector in the magnetic field direction) and assume a time dependent solution to be implemented by an implicit scheme, we illustrate it in the following for the steady state case, where we just balance the divergence of the heat flux against the volumetric sources Q.

In an isotropic case, the lowest order conservative finite difference formulation of the heat conduction operator is

$$\nabla \cdot \vec{q} = \left[\frac{1}{\Delta x}\left(q_{x,i+\frac{1}{2},j} - q_{x,i-\frac{1}{2},j}\right) + \frac{1}{\Delta y}\left(q_{y,i,j+\frac{1}{2}} - q_{y,i,j-\frac{1}{2}}\right)\right], \tag{3}$$

with

$$\begin{aligned} q_{x,i+\frac{1}{2},j} &= -\frac{(n\chi)_{i+\frac{1}{2},j}}{\Delta x}(T_{i+1,j} - T_{i,j}), \\ q_{y,i,j+\frac{1}{2}} &= -\frac{(n\chi)_{i,j+\frac{1}{2}}}{\Delta y}(T_{i,j+1} - T_{i,j}), \end{aligned} \tag{4}$$

etc., where we have adopted a grid labelling (Fig. 1) with temperatures defined at integer points.

Adding anisotropy to it, requires in addition the knowledge of the temperature gradient $\frac{\partial}{\partial y}T|_{i+\frac{1}{2},j}$ and equivalent terms, which, in the most straightforward manner can be written as

$$\left.\frac{\partial}{\partial y}T\right|_{i+\frac{1}{2},j} = \frac{1}{4(\Delta y)}\left((T_{i+1,j+1} + T_{i,j+1}) - (T_{i+1,j-1} + T_{i,j-1})\right), \tag{5}$$

which clearly implies a significant difference in the evaluation of the gradients in the two directions. We will label this scheme therefore "asymmetric" in the following.

A more symmetric formulation is obtained by first expressing both components of the temperature gradients (and subsequently of the total parallel heat flux $\vec{q}_{\parallel} = \vec{b}n\chi_{\parallel}(\vec{b}\cdot\nabla T)$) by the function values at the same grid points

$$\left.\frac{\partial}{\partial x}T\right|_{i+\frac{1}{2},j+\frac{1}{2}} = \frac{1}{2(\Delta x)}\left((T_{i+1,j+1} + T_{i+1,j}) - (T_{i,j+1} + T_{i,j})\right), \tag{6a}$$

$$\left.\frac{\partial}{\partial y}T\right|_{i+\frac{1}{2},j+\frac{1}{2}} = \frac{1}{2(\Delta y)}\left((T_{i+1,j+1} + T_{i,j+1}) - (T_{i+1,j} + T_{i,j})\right), \tag{6b}$$

and

$$q_{\parallel,x,i+\frac{1}{2},j+\frac{1}{2}} = -(n\chi_{\parallel}b_x)_{i+\frac{1}{2},j+\frac{1}{2}}\left(b_{x,i+\frac{1}{2},j+\frac{1}{2}}\cdot\left.\frac{\partial}{\partial x}T\right|_{i+\frac{1}{2},j+\frac{1}{2}} + b_{y,i+\frac{1}{2},j+\frac{1}{2}}\cdot\left.\frac{\partial}{\partial y}T\right|_{i+\frac{1}{2},j+\frac{1}{2}}\right), \tag{7a}$$

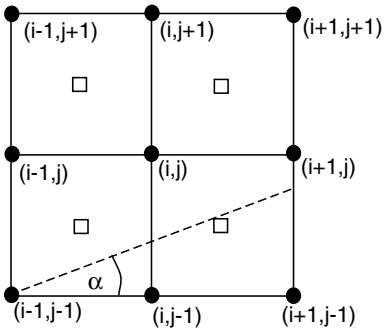

Fig. 1. Grid labelling and elementary cell.

$$q_{\parallel,y,i+\frac{1}{2},j+\frac{1}{2}} = -(n\chi_\parallel b_y)_{i+\frac{1}{2},j+\frac{1}{2}}\left(b_{x,i+\frac{1}{2},j+\frac{1}{2}}\cdot\frac{\partial}{\partial x}T\bigg|_{i+\frac{1}{2},j+\frac{1}{2}} + b_{y,i+\frac{1}{2},j+\frac{1}{2}}\cdot\frac{\partial}{\partial y}T\bigg|_{i+\frac{1}{2},j+\frac{1}{2}}\right), \tag{7b}$$

and expressing the divergence of the parallel heat flux as:

$$\nabla\cdot\vec{q}_\parallel\big|_{i,j} = \frac{1}{2(\Delta x)}\left(q_{\parallel,x,i+\frac{1}{2},j+\frac{1}{2}} + q_{\parallel,x,i+\frac{1}{2},j-\frac{1}{2}} - q_{\parallel,x,i-\frac{1}{2},j+\frac{1}{2}} - q_{\parallel,x,i-\frac{1}{2},j-\frac{1}{2}}\right) + \frac{1}{2(\Delta y)}\left(q_{\parallel,y,i+\frac{1}{2},j+\frac{1}{2}} + q_{\parallel,y,i-\frac{1}{2},j+\frac{1}{2}} - q_{\parallel,y,i+\frac{1}{2},j-\frac{1}{2}} - q_{\parallel,y,i-\frac{1}{2},j-\frac{1}{2}}\right). \tag{8}$$

Both the asymmetric and the symmetric schemes can be shown to be conservative, however only the symmetric scheme corresponds to a difference formulation of the operators div and grad which maintains the self-adjointness of the operator $\nabla\cdot\chi_\parallel(\vec{b}\cdot\nabla T)\vec{b}$ in the discretised form. In fact, the scheme in this form can be viewed as a special application of the support-operator algorithm described in [15].

Numerical errors for the solution of the anisotropic heat conduction equation in the limit of large $\chi_\parallel/\chi_\perp$ should have two effects: (1) the appearance of unphysical temperature gradients along field lines, and (2) a finite heat flux perpendicular to field lines, proportional, at given temperature gradients, to $\chi_\parallel$. Both effects can be studied and separated by the solution of a test case, where we solved the steady-state version of Eqs. (1) and (2) over the interval $-0.5 \leqslant x, y \leqslant 0.5$, for a magnetic field with circular flux surfaces centred either at x_0,$y_0 = -0.5$ (open field line case) or x_0,$y_0 = 0$ (mainly closed field line case). Heat sources and Dirichlet boundary conditions were chosen so as to correspond to the solution $T(r) = 1 - r^3$, with $r = \sqrt{(x-x_0)^2 + (y-y_0)^2}$, and $\chi_\perp$ was normalised to 1. The error scaling for the two schemes (Fig. 2) shows a marked difference between the open and the closed field line cases. In the open field line case,

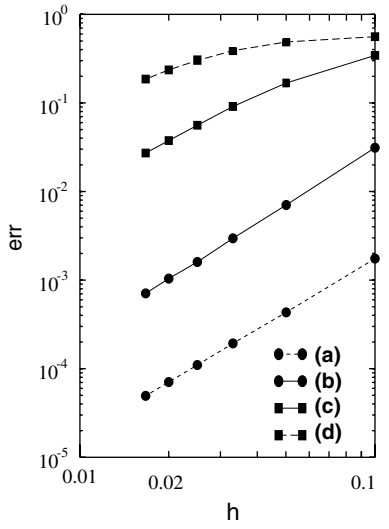

Fig. 2. Scaling of error, given by err = $|T^{\text{num}}(0,0) - T^{\text{anal}}(0,0)|/|T^{\text{anal}}(0,0) - T^{\text{anal}}(-0.5,0)|$, of the symmetric and asymmetric schemes with grid spacing h and different values of $\chi_\parallel(\chi_\perp = 1$, throughout), for circular flux surfaces, for field configurations with either all field lines intersecting the boundary ($x_0 = y_0 = -0.5$) or predominantly closed field lines ($x_0 = y_0 = 0$). Results of the symmetric scheme for values of $100 \leqslant \chi_\parallel < 10^9$ (not shown) for both configurations are indistinguishable on scale of this plot. Also not shown is the error of asymmetric scheme for the case of all field lines intersecting the boundary, which is even below that of the symmetric scheme: (a) symmetric scheme, $x_0 = y_0 = -0.5$, $\chi_\parallel = 10^9$, (b) symmetric scheme, $x_0 = y_0 = 0$, $\chi_\parallel = 10^9$, (c) asymmetric scheme, $x_0 = y_0 = 0$, $\chi_\parallel = 10^2$, (d) asymmetric scheme, $x_0 = y_0 = 0$, $\chi_\parallel = 10^3$.

the errors for both schemes are very small and practically independent of $\chi_\parallel$. In this case all field lines intersect the boundary, and both schemes succeed in enforcing $T = \text{const.}$ along field lines, so that the solution becomes dominated by the boundary conditions. In the case with mainly closed field lines, the field lines still remain to high accuracy isotherms, but the perpendicular gradient becomes strongly affected by pollution due to the spurious perpendicular heat fluxes. Whereas the symmetric scheme shows, up to the tested limit of $\chi_\parallel = 10^9$, an error independent of $\chi_\parallel$ (dominated by the discretisation error of the true perpendicular heat flux proportional to $\chi_\perp$), the error for the asymmetric scheme is clearly dominated by pollution, increasing, in the non-saturated regime, proportionally to $\chi_\parallel$.

Magnetic geometries of practical interest for plasma transport calculations require, in general, a non-orthogonal coordinate system in the poloidal plane. To test, whether additional errors will arise in this case, we have repeated the calculations for the closed flux surface geometry in non-orthogonal (albeit Cartesian) coordinates, defined by $x^1 = x - y\frac{\cos\alpha}{\sin\alpha}$, $x^2 = y\frac{1}{\sin\alpha}$, with Dirichlet boundary conditions defined along the boundaries of the computational region: $-\frac{1}{2\sin\alpha} \leqslant x^1$, $x^2 \leqslant \frac{1}{2\sin\alpha}$. The latter was chosen so as to be tangent to the same flux-surface as the orthogonal case, taking into consideration the importance of the closed flux surface region. Decreasing α, at constant number of grid points we expect a trivial increase in error due to the reduced number of useful grid points (namely those in the closed flux surface region). An additional error might arise due to the response of the scheme to the non-orthogonality of the grid.

Results reported here refer to a source distribution giving $T(r) = \exp(-(r/4)^2)$ as analytic solution, having – except in individual points – non-vanishing derivatives to all orders. At given number of grid points $N = N_{x^1} = N_{x^2}$, the error of the symmetric scheme indeed increases with decreasing α, remaining virtually independent of $\chi_\parallel/\chi_\perp$ (Fig. 3). It depends, however, much weaker on angle than the ''asymmetric scheme'', whose error is smaller in the isotropic case with $\alpha = \pi/2$, but increases more strongly with decreasing α, and even dramatically with increasing $\chi_\parallel/\chi_\perp$. In fact, the error of the symmetric scheme can be fully attributed to the loss of resolution at given N: plotting it against $\Delta x^1 = \Delta x^2$ the points for different values of α lie on a universal line (Fig. 4). This is to be expected as the error (being quadratic in distance between points) will be dominated by the distance of grid points in the least resolved direction, which in this case is proportional to $1/\sin\alpha$. Remarkable is the fact that for all angles the error of the extremely anisotropic case $\chi_\parallel/\chi_\perp = 10^9$ (shown in Fig. 4) remains close to that of the isotropic one.

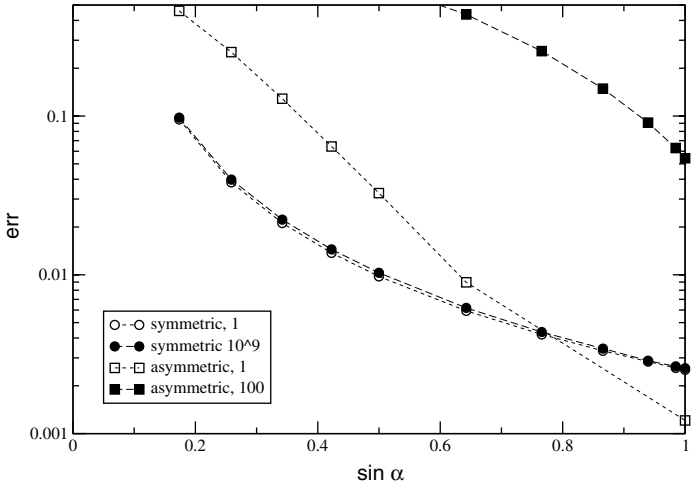

Fig. 3. Error of calculations using non-orthogonal coordinates for the closed field line case of Fig. 2, as function of $\sin\alpha$, for $N = 58$. Results given refer to the symmetric scheme using $\chi_\parallel/\chi_\perp = 1$ and 10^9, and to the asymmetric scheme for $\chi_\parallel/\chi_\perp = 1$ and 10^2.

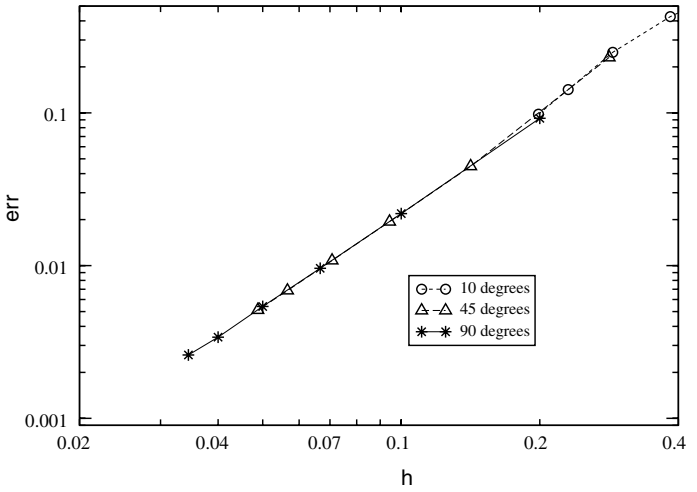

Fig. 4. Error of calculations using non-orthogonal coordinates for the closed field line case of Fig. 2, as function of grid spacing $h = \Delta x^1 = \Delta x^2$ for three different values of α, for the symmetric scheme with $\chi_\parallel/\chi_\perp = 10^9$.

The favourable pollution control feature of the symmetric scheme also holds in more general geometry (including, in particular also a mix of concave and convex field line regions and an X-point). Taking a 2-d magnetic field configuration derived from a flux function as $\vec{B} = \vec{e}_z \times \nabla\psi$, and choosing a heat source satisfying $Q(x,y) = -\chi_\perp \nabla^2 \psi(x,y)$, ensures, together with appropriate boundary conditions, that the true solution will be a constant on field lines, irrespective of the value of $\chi_\parallel/\chi_\perp$ [9]. This test case is also of interest, as it corresponds to a situation of finite divergence of the magnetic direction vector $\nabla \cdot \vec{b}$. The function chosen for $\psi(x,y)$, $T(x,y)$ was $\sin(2\pi x) \cdot \cos(2\pi y)$, over the interval $-0.5 \leqslant x,y \leqslant 0.5$. Fig. 5(a) and (b) show the results of the symmetric and the asymmetric scheme for the case imposing the analytic solution at the boundary as Dirichlet type condition. Whereas the symmetric scheme reproduced the true solution accurately over the whole region, again independently of $\chi_\parallel$, the asymmetric scheme does so only over the region covered by field lines intersecting the boundary, flattening T nearly completely over the region of closed field lines. Imposing periodic (rather than Dirichlet type) boundary conditions leaves the solution obtained with the symmetric scheme essentially unchanged, but flattens T in the asymmetric case now over the *whole* computational region. We have compared our error scaling and its dependence on the ratio $\chi_\parallel/\chi_\perp$ also with the very extensive tests carried out by the *NIMROD*-Team for different order finite element representations. For these cases the region used is again the unit square $-0.5 \leqslant x,y \leqslant 0.5$, with sources appropriate to produce $\psi(x,y), T(x,y) \sim \cos(\pi x) \cdot \cos(\pi y)$, and Dirichlet boundary conditions. The results of these tests, and the comparison with the finite element results of [9] are shown in Fig. 6(a)–(c) for ratios $\chi_\parallel/\chi_\perp = 10^3$, 10^6, 10^9. The results of the "symmetric" finite difference scheme also for this case show a pronounced h^2 scaling, but are also virtually independent of the conductivity anisotropy. As consequence, for the largest $\chi_\parallel/\chi_\perp$-values the present scheme not only outperforms the bilinear and bi-quadratic schemes, but even behaves better than the bi-cubic finite element model.

3. Combined finite-difference and fourier representation for the 3-d case

Multi-dimensional heat transport problems in toroidal confinement systems generally originate from perturbations of initially closed, nested flux surfaces. It is therefore appropriate to exploit this feature also

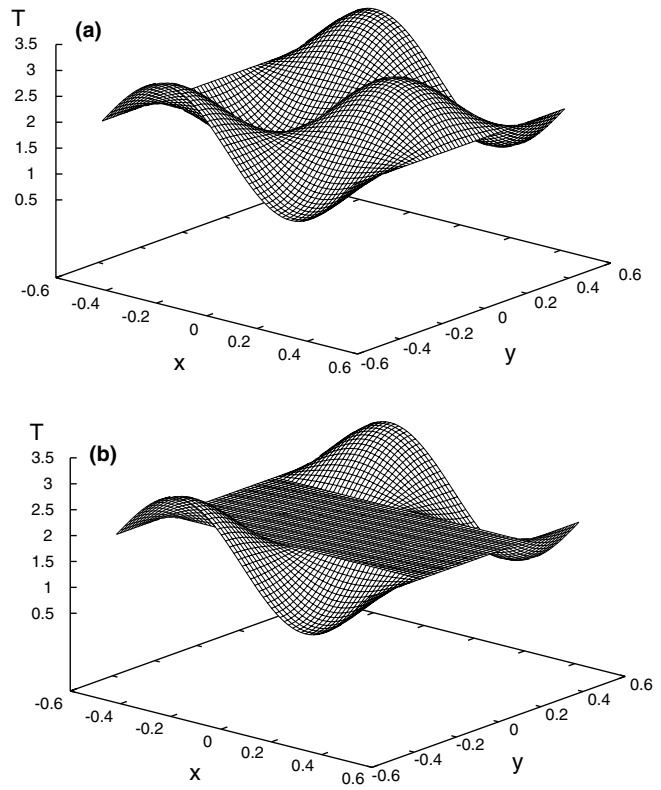

Fig. 5. Numerical solution for analytic test case with a magnetic field defined by flux function $\psi(x, y) = \sin(2\pi x) \cdot \cos(2\pi y)$, for $\chi_{\|}/\chi_{\perp} = 10^9$, with Dirichlet boundary conditions on a 60×60 grid. (a) Symmetric Scheme, (b) asymmetric scheme.

in the choice of coordinate system. The simplest, topologically relevant configuration is a "periodic" straight cylinder, with an unperturbed field given by

$$\vec{B}_o = B_{ot}\left(\vec{e}_z + \frac{r}{qR}\vec{e}_\theta\right) = B_{ot}\left(\vec{e}_z - \frac{nr}{mR}\vec{e}_\theta\right) + \nabla\psi_0(r) \times \vec{e}_z \tag{9}$$

in cylindrical coordinates r, θ, z. The "safety factor" $q(r)$ here determines the pitch angle of the field lines and the periodicity length $2\pi R$ describes the lowest order torus effect. In the framework of reduced MHD [16,17], magnetic perturbations to this configurations can be described in terms of a helical flux function ψ as

$$\vec{B} = \vec{B}_o + \nabla \sum_j \psi_j(r) \exp \mathrm{i}\left(m_j\theta + \frac{n_j}{R}z\right) \times \vec{e}_z, \tag{10}$$

neglecting perturbations in the toroidal field. The time-dependent, 3-d, non-linear simulation of neoclassical tearing modes in this configuration and with these coordinates had, in fact been the original driver of our code development. The periodicity requirements and the chosen representation of the magnetic field suggest to use a Fourier ansatz in θ and $\phi = z/R$ also for the solution of the heat conduction equation.

In this section, we outline the scheme used in this case at hand of a very simplified model, which makes more transparent the steps taken to reduce the pollution of the perpendicular heat fluxes by parallel ones. The full algebra for the general case, needed also for the applications described later in this section, is

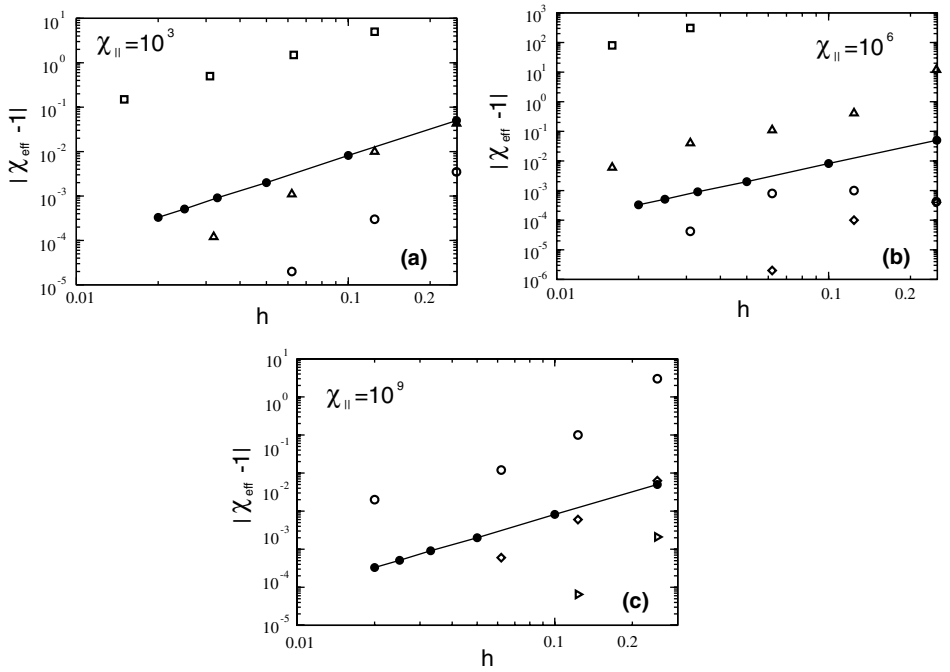

Fig. 6. Scaling of error for the analytic test case with grid spacing for the symmetric scheme, compared with results of [9] using finite element formulations, for values of $\chi_\parallel/\chi_\perp = 10^3$ (a), 10^6 (b), 10^9 (c). Note the virtual independence of the error of the symmetric scheme from the heat conductivity anisotropy (symmetric finite difference scheme: connected dots; bilinear elements: □, bi-quadratic: △, bi-cubic: ○, bi-quartic: ◆, bi-quintic: ▷).

shifted to the appendix. The simple model assumes a magnetic field perturbation with a single helicity $\vec{B}_1 = \nabla\psi_1(r)\exp \mathrm{i}(m_1\theta + n_1\phi) \times \vec{e}_z$. Assuming that heat sources and sinks also respect this symmetry, also the temperatures will vary with θ,ϕ only with this combination of m_1, n_1 and integer multiples. For constant heat conductivities and plasma densities, the lowest order equations in a Fourier expansion will read

$$\frac{3}{2}\frac{\partial}{\partial t}T_0 - \chi_\perp \nabla_\perp^2 T_0 - Q_0 = \frac{1}{2}\left(\chi_\parallel \vec{b}_1^* \cdot \nabla(\vec{b}_1 \cdot \nabla T_0 + \vec{b}_0 \cdot \nabla T_1) + \text{c.c.}\right), \tag{11}$$

$$\frac{3}{2}\frac{\partial}{\partial t}T_1 - \chi_\perp \nabla_\perp^2 T_1 = \chi_\parallel \vec{b}_0 \cdot \nabla(\vec{b}_1 \cdot \nabla T_0 + \vec{b}_0 \cdot \nabla T_1), \tag{12}$$

where the index 0 for T refers to the θ,ϕ-independent part (generally not identical with the unperturbed equilibrium).

This formulation allows to illustrate very well the danger of cutting-off the Fourier expansion at a given order of T_j. Including only T_0, the magnetic field perturbation would produce (using a prime to express radial derivatives) a term $\approx \chi_\parallel b_{1r}^2 T_0''$ in Eq. (11), which for realistic perturbation amplitudes ($|B_1| \approx \mathrm{O}(10^{-4}|B_0|)$) and heat-conductivity ratios could easily swamp the perpendicular heat conductivity contribution in the determination of the flux-surface averaged temperature profile. In reality, however, a variation T_1 will appear along the unperturbed field-line direction $\vec{b}_0$, trying to keep the temperature constant along the actual, perturbed field line. Solving simultaneously Eqs. (11) and (12) for T_0 and T_1 will allow the latter to adjust, so as to produce this cancellation, and will leave only an order of magnitudes

smaller net effect upon the radial variation of the averaged profile. Proceeding to higher orders (see appendix and test case reported in Fig. 12) we implement this concept by terminating the expansion at a given order of the gradients along field lines rather than of the temperature. Eq. (11) also illustrates that in this configuration, realistic for toroidal confinement systems, the projection of the field lines onto the poloidal plane determines the danger of pollution of perpendicular transport, so that $(\chi_\parallel B_{\mathrm{pol}}^2)/(\chi_\perp B_{\mathrm{tor}}^2)$ rather than $\chi_\parallel/\chi_\perp$ like in the 2-d case is the relevant parameter to measure the challenge to the numerical scheme.

Pursuing this concept further it becomes evident that in order to allow the cancellation of spurious temperature differences along field lines, it is important to ensure that also in the discretised form, the temperature gradients along field lines, should appear in the same form (i.e. involving the same grid points) in Eqs. (11) and (12). This would not be ensured by the most straightforward discretisation, which would result (using $T_i(r)$ now only for the radially depending Fourier coefficient and substituting $\vec{b}_0 \cdot \nabla$ by $\mathrm{i}(\vec{k} \cdot \vec{b}_0)$; for transparency we also use here constant $\vec{b}_0, \vec{b}_1$), for the RHS terms in Eqs. (11) and (12), in

$$\vec{b}_1^* \cdot \nabla(\vec{b}_1 \cdot \nabla T_0 + \vec{b}_0 \cdot \nabla T_1) = \frac{b_{1,r}^*}{\Delta r} \begin{pmatrix} \frac{b_{1,r}}{\Delta r}(T_0^{i+1} - T_0^i) + \frac{\mathrm{i}(\vec{k}\cdot\vec{b}_0)^{i+1/2}(T_1^{i+1}+T_1^i)}{2} \\ -\left(\frac{b_{1,r}}{\Delta r}(T_0^i - T_0^{i-1}) + \frac{\mathrm{i}(\vec{k}\cdot\vec{b}_0)^{i-1/2}(T_1^i+T_1^{i-1})}{2}\right) \end{pmatrix}, \tag{13}$$

$$\vec{b}_0 \cdot \nabla(\vec{b}_1 \cdot \nabla T_0 + \vec{b}_0 \cdot \nabla T_1) = \mathrm{i}(\vec{k} \cdot \vec{b}_0)\left(\frac{b_{1,r}}{2\Delta r}(T_0^{i+1} - T_0^{i-1}) + \mathrm{i}(\vec{k} \cdot \vec{b}_0)T_1^i\right). \tag{14}$$

Substituting, however, Eq. (14) by

$$\vec{b}_0 \cdot \nabla(\vec{b}_1 \cdot \nabla T_0 + \vec{b}_0 \cdot \nabla T_1) = \mathrm{i}(\vec{k} \cdot \vec{b}_0)^i \begin{pmatrix} \frac{b_{1,r}}{2\Delta r}(T_0^{i+1} - T_0^{i-1}) + \\ \frac{\mathrm{i}(\vec{k}\cdot\vec{b}_0)^{i+1/2}(T_1^{i+1}+T_1^i)}{4} + \frac{\mathrm{i}(\vec{k}\cdot\vec{b}_0)^{i-1/2}(T_1^i+T_1^{i-1})}{4} \end{pmatrix}, \tag{15}$$

conserves the order of truncation error, but allows the difference formulations (13) and (15) to be cast into the form

$$\ldots = \frac{b_{1,r}^*}{\Delta r}(\alpha - \beta)$$
$$\ldots = \frac{\mathrm{i}(\vec{k} \cdot \vec{b}_0)^i}{2}(\alpha + \beta),$$

respectively, with

$$\alpha = \frac{b_{1,r}}{\Delta r}(T_0^{i+1} - T_0^i) + \frac{\mathrm{i}(\vec{k} \cdot \vec{b}_0)^{i+1/2}}{2}(T_1^{i+1} + T_1^i),$$
$$\beta = \frac{b_{1,r}}{\Delta r}(T_0^i - T_0^{i-1}) + \frac{\mathrm{i}(\vec{k} \cdot \vec{b}_0)^{i-1/2}}{2}(T_1^i + T_1^{i-1}).$$

This allows, if the terms arising from sources, time derivatives and perpendicular heat conduction exactly balance, the total parallel temperature gradients to vanish simultaneously at both intermediate points $i + 1/2, i - 1/2$. This feature, which is analogous to the principle applied in Section 2, is conserved also for variable $\vec{b}$ (see expressions given in appendix), and turns out to be essential for the strongly reduced pollution of the scheme presented here.

We have implemented these principles in a code allowing for arbitrary multi-helicity perturbations to the magnetic field and consequently also the temperatures. The details of the scheme are outlined in the appendix. In the following we present a series of increasingly realistic and relevant test calculations conducted with this code.

3.1. Comparison with analytic test cases

A simple analytic test case, constituting an extension of the one used in Section 2, can be constructed assuming a single helicity perturbation of the magnetic field ψ_1 and choosing the power deposition profile so that $Q(r,\theta,\phi) = -\chi_\perp \nabla^2 \psi$. With appropriate boundary conditions this ensures $T = T(\psi)$ and hence $\nabla_\parallel T = 0$ as a stationary solution. In a non-aligned coordinate system, like used here, this constitutes a non-trivial test case. For the following tests we have chosen the equilibrium helical flux to be $\psi_0(r) = \psi_{0a}(r/a)^2((r - r_s)/a)^2$, $\psi_{0a} = 10^{-1} a B_{0t}$, $r_s = 1.2a$ and a single field perturbation with the helicity $(m,n) = (3,2)$ given by $\psi_1(r) = \psi_{1a}(r/a)^2$, $\psi_{1a} = 10^{-3} a B_{0t}$.

Fig. 7 shows the difference between the numerical results using a simple second order scheme according to Eq. (14) – labelled "asymmetric" in the following – and the analytical solution $T = \psi$ of the heat transport equation at half the plasma minor radius

$$\mathrm{Err}(0,0) = \log_{10}\left[\frac{T_{\mathrm{numerical}} - T_{\mathrm{analytical}}}{T_{\mathrm{analytical}}}\right]_{(m,n)=(0,0)}^{r=0.5a}$$

versus the number of radial grid points for three values of $\chi_\parallel/\chi_\perp$. Here, we use for the purpose of illustration an equidistant grid, although, in general, only the step size in a narrow region (the proximity of islands) is determinant. As expected the numerical error scales like $(\Delta r)^2$, and is dominated, for sufficiently high values of $\chi_\parallel/\chi_\perp$ by the parallel conduction term. In fact, over a significant range it increases linearly with $\chi_\parallel$ as expected from the discussion in Section 2. The association of the error with the 3rd and higher derivatives of T_j can be also verified by selecting $\psi_0(r) = \psi_{0a}(r/a)^2$ (other conditions unchanged), which makes these derivatives vanish. In this case even 50 grid points suffice to bring $\log_{10}[\mathrm{Err}(0/0)]$ down to -11, for $\chi_\parallel/\chi_\perp = 10^9$.

In this analytic example it is transparent that the numerical error derives essentially from the inability of the numerical scheme to relax the T_j^i so as to make parallel gradients and hence parallel heat fluxes vanish. Our modified scheme (using the expressions given in the appendix, following the ideas presented in the derivation of Eq. (15)) can do this, and should therefore behave particularly well in this test. In fact, Fig. 8 shows that its numerical error for this case is dominated by the $\chi_\perp$-contribution, remaining independent of $\chi_\parallel/\chi_\perp$ up to (unrealistic) values $\geqslant 10^{14}$, and equal to the one of the ordinary scheme for very small $\chi_\parallel/\chi_\perp$. It scales again like $1/N^2$, and its independence from the parallel conductivity holds also for the higher Fourier components.

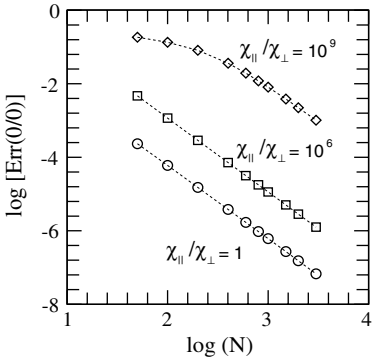

Fig. 7. Logarithmic ($\log_{10}$) representation of error in the $(0,0)$ component of T for the "asymmetric" numerical scheme applied to the analytic test case, as function of the number of (equidistant) grid points N, for values of $\chi_\parallel/\chi_\perp = 1$, 10^6, 10^9. Number of Fourier components: 40.

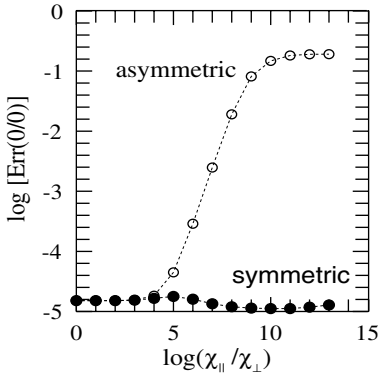

Fig. 8. Error in the (0,0) component of T of the "asymmetric" and the "symmetric" schemes for the analytic test case as function of $\chi_\parallel/\chi_\perp$, for 200 grid points and 40 Fourier components.

3.2. Tests for general single-helicity cases

The above test case is particularly favourable to our scheme. In many important applications involving magnetic islands, however, a thin transition layer develops around the separatrix region whose width is determined by the competition of parallel and perpendicular heat fluxes. For a more realistic test, we use therefore an unperturbed q-profile given by $q(r) = 0.86(1 + (2r/a)^4)^{1/2}$, and a perturbed flux varying like either $\Psi_{(3,2)}(r) = 10^{-3}aB_{0t}(r/a)^2(1 - r/a)^2$, leading to the formation of a magnetic island of the width $0.059a$ at the $q = 3/2$ rational surface at about $r_s \sim 0.6a$, or like $\Psi_{(2,4)}(r) = 10^{-3}aB_{0t}(r/a)^2(1 - r/a)^2$ with no resonance in the plasma. The power source is specified as $Q_0(r) = -\chi_\perp\nabla^2(0.95(1 - (r/a)^2)^4 + 0.05)$. As reference for the estimation of the numerical error we use in these cases – for which no analytic solutions exist – the results of the symmetric scheme with 9000 grid points and 85 Fourier components.

A significant difference exists in the performance of our scheme in the two respective cases (Fig. 9). Although in both cases its performance is much better than that of the "asymmetric" scheme at high values of $\chi_\parallel/\chi_\perp$ the deterioration of performance at given N with increasing parallel heat conductivity sets in (for

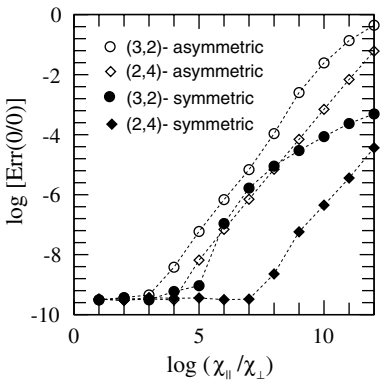

Fig. 9. Error in the (0/0) component of T of the "asymmetric" and the "symmetric" schemes for two test cases corresponding to magnetic perturbations resonant inside the plasma (3/2 case) or not (2/4 case), respectively as function of $\chi_\parallel/\chi_\perp$, for 2000 grid points and 85 Fourier components.

the given N-value) about a factor of 100 earlier in the island-dominated case. The origin of the deterioration in the resonant case can be traced to the necessity to resolve the singular layer, and becomes evident in the dependence of the error of the resonant (3/2) component of the temperature on N, for a given $\chi_\parallel/\chi_\perp$ (Fig. 10). In case of a magnetic island one has to ensure that the width in which the parallel heat transport does not vanish is well resolved. This is the critical island width [14] $w_c = a(\chi_\perp/\chi_\parallel)^{1/4}(\varepsilon s n/8)^{-1/2}$ (with $s = (r/q)\mathrm{d}q/\mathrm{d}r$ and $\varepsilon = r/R$) for small islands ($w < w_c$) and w_c^2/w for $w > w_c$. In our case we therefore have to resolve $w_c^2/w = 1.2 \times 10^{-2}a$ for $\chi_\parallel/\chi_\perp = 10^8$, and $3.6 \times 10^{-3}a$ for $\chi_\parallel/\chi_\perp = 10^9$. Fig. 10 shows that if less than 3 points are located in the region w_c^2/w the numerical error significantly increases. This is evidently a truly physical limitation which should be countered by a suitable accumulation of grid points in the relevant space region. Also shown in this Fig. 10 is a case with spatially variable ratio $\chi_\parallel/\chi_\perp$, with an assumed variation $\chi_\parallel/\chi_\perp = (\chi_\parallel/\chi_\perp)_o/\sqrt{1 + c_1^2(\vec{k}\cdot\vec{b}_o)^2}$ approximating the effect of a correction to the Spitzer heat conductivity for finite wave number of the temperature perturbation along the magnetic field [12]. For the case in Fig. 10 $(\vec{k}\cdot\vec{b}_o) = r_s/R(2/3 - r/(r_s q))$, $(\chi_\parallel/\chi_\perp)_o = 10^9$ and $c_1 = 1000$ were used. This variable heat conductivity case also behaves as expected, showing a transition to the well-resolved regime at a value of N lower than would correspond to $(\chi_\parallel/\chi_\perp)_o$.

Local accumulation of grid points in the island region is particularly indicated for this problem, and we have therefore chosen it as a test case for the response of the scheme to variable mesh size. The simple method of using a discontinuous reduction from of Δr to $\Delta r/N^*$ (integer N^*) inside an interval $r_s - \delta \leqslant r \leqslant r_s + \delta$ worked well, provided the jump occurred in a region of small $\left|\frac{\mathrm{d}^2}{\mathrm{d}r^2}T_{(m,n)}\right|$, i.e. far enough away from the island. A more flexible scheme, however, consists in the introduction of a coordinate transformation to a coordinate ρ, with $\mathrm{d}r/\mathrm{d}\rho \to 1$ in the uncritical, and $\mathrm{d}r/\mathrm{d}\rho \ll 1$ in the regions requiring high resolution, and the use of an equidistant grid in ρ. Fig. 11 shows the results of this method for the test problem for a (spatially constant) value of $\chi_\parallel/\chi_\perp = 10^{10}$ and the coordinate transformation $\mathrm{d}r/\mathrm{d}\rho = 1 - a_1\{\exp(-((r/a - 0.47)/0.065)^2) + \exp(-((r/a - 0.56)/0.065)^2)\}$. The cases plotted correspond to a constant interval size $\Delta r = 1/200$ away from the island region. Plotting cases with different a_1 against the inverse of the minimum of Δr: $N_{\mathrm{eff}} = 1/(\Delta r)_{\min}$ shows indeed a close agreement to the results of the homogeneously spaced case with $N = N_{\mathrm{eff}}$ up to a certain value of N_{eff}, beyond which no improvement occurs in the inhomogeneous grid case, as the error is now dominated by the residual error in the region outside the island, where the resolution is kept fixed.

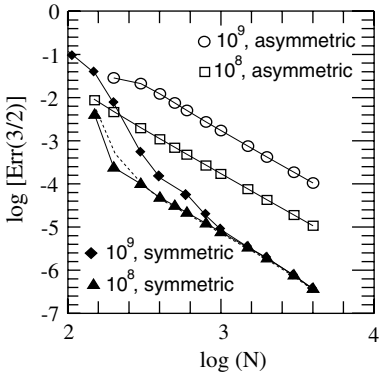

Fig. 10. Error in the (3/2) component of T for a resonant (3/2) test case ($q(r) = 1.025(1 + (2r/a)^4)^{1/2}$, $\psi_{3,2}(r) = 6 \times 10^{-4}aB_{0t}(r/a)^2(1 - r/a)^2$), as function of grid point number N, for the asymmetric and the symmetric schemes for different values of $\chi_\parallel/\chi_\perp$. Number of Fourier components used: 85. Also shown is a case with spatially variable parallel heat conductivity, with $(\chi_\parallel/\chi_\perp)_0 = 10^9$, $c_1 = 10^3$ (dotted line).

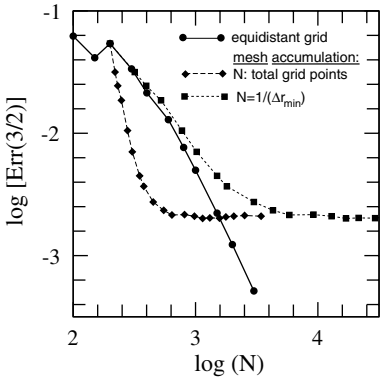

Fig. 11. Error in the (3/2) component of T for the resonant (3/2) test case of Fig. 9, as function of grid point number N, for the symmetric scheme for $\chi_\parallel/\chi_\perp = 10^{10}$ using equidistant grid and mesh accumulation. The results for the latter case are given both as function of total grid points N and as function of the inverse of the minimum grid spacing $N_{\text{eff}} = 1/(\Delta r)_{\min}$. Number of Fourier components: 85.

In all above test cases we have applied the strategy to cut-off the Fourier components at a given consistent order in parallel heat flux (rather than temperature). Fig. 12 shows the consequences of implementing or not this scheme, again for the resonant ((3/2)-perturbation) test case of Fig. 9.

3.3. Application to multiple helicity perturbations

The sample applications given above refer to magnetic perturbations with a single helicity. As is shown in the appendix, the method can, however, be readily extended to cases with several Fourier components and hence to situations where cross-field transport interacts with multiple secondary islands and incipient ergodisation. As an example we consider here simultaneous field perturbations given by $\Psi_{(3,2)}(r) = 2\times10^{-4}B_{0t}(r/a)^2(1-r/a)^2$ and $\Psi_{(4,3)}(r) = 2\times10^{-4}B_{0t}(r/a)^2(1-r/a)^2$ in an equilibrium field with $q = 0.2\exp(r/(0.3a))$, leading to primary islands at the (3/2) and (4/3) surfaces in the plasma. For the chosen perturbation amplitudes these primary islands do not overlap. Secondary islands appear, however, at the m/n = 7/5, 10/7 and 11/8 surfaces as evidenced by the Poincare plot of the magnetic field lines (Fig. 13) and an ergodic region starts to develop around the separatrix of the 4/3 island.

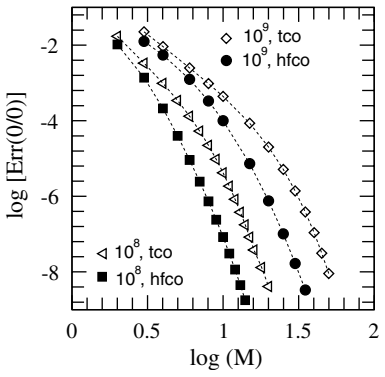

Fig. 12. Effect of different cut-off strategies in the Fourier decomposition. Error in the (0/0) component of T for the (3/2) test case of Fig. 9 (with a resonance inside the plasma region), as function of Fourier components included, for the heat flux (hfco) and the temperature (tco) cut-off strategy, respectively, for two different values of $\chi_\parallel/\chi_\perp$. The radial discretisation corresponds to the symmetric scheme for both cases; 1600 grid points are used.

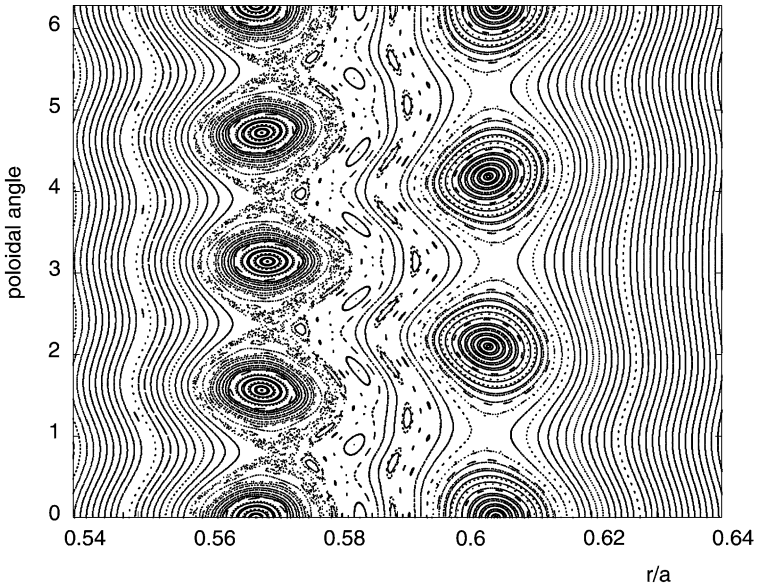

Fig. 13. Poincare plot of the field line intersection points with the r,θ plane at $\phi = 0$ for the case of a perturbation field with two helicities (m/n = 3/2 and 4/3).

Solving the heat transport equation in this field geometry with a source distribution given by $Q = -\chi_\perp \nabla^2((1-(r/a)^2)^8(r/a)^8)$ shows that still a visible difference exists in the temperature iso-contours between a case with $\chi_\parallel/\chi_\perp = 10^{10}$ (Fig. 14) and one with $\chi_\parallel/\chi_\perp = 10^{12}$ (Fig. 15) and that it can be resolved by our code: the 7/5 island appears visible as such only in the higher parallel conductivity situation. More details on this case and other applications will be given in a follow-up paper.

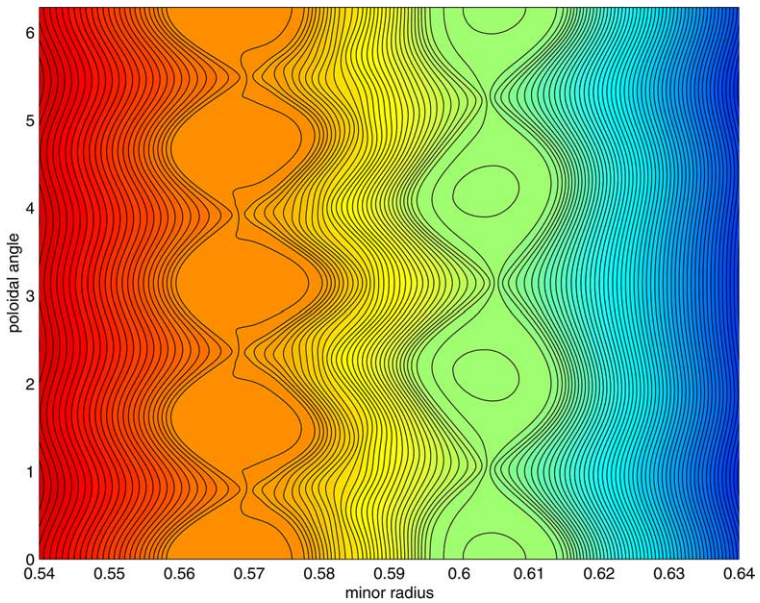

Fig. 14. Temperature iso-contours for the magnetic field of Fig. 13 and a ratio of $\chi_\parallel/\chi_\perp = 10^{10}$ (corresponding, e.g. to $\chi_\perp = 1\ \mathrm{m^2/s}$ and $\chi_\parallel = \chi_{\mathrm{Spitzer}}$ for $T_e = 1.2$ keV, $n_e = 5\times 10^{19}\ \mathrm{m^{-3}}$).

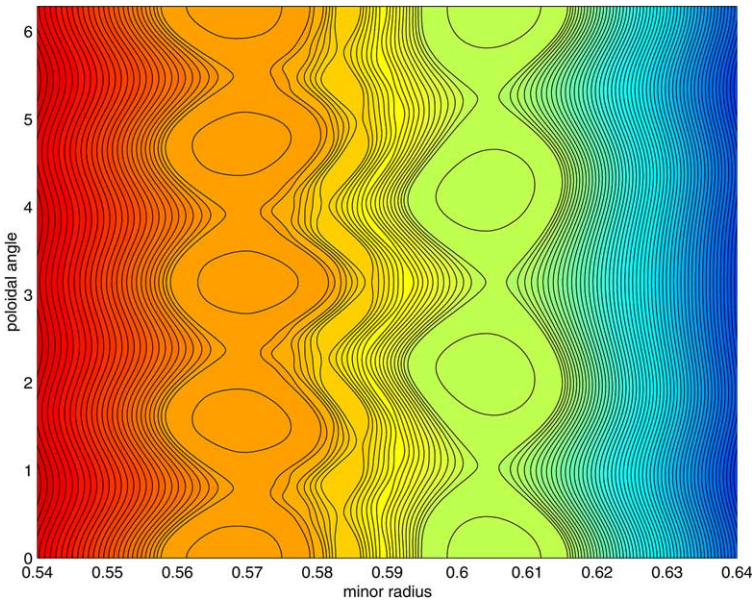

Fig. 15. Temperature iso-contours for the magnetic field of Fig. 13 and a ratio of $\chi_{\|}/\chi_{\perp} = 10^{12}$.

4. Conclusions

The symmetric difference schemes outlined above hold promise to control the numerical pollution of true perpendicular heat conduction by numerical, parallel conductivity driven transport over a significant parameter range. They appear particularly attractive for dynamic calculations, where the implementation of exact alignment of the coordinate system with the field would be very time-consuming or – when closed flux surfaces cease to exist – even impossible, and where the required accuracy is limited by the co-existence of other strong effects. Transport calculations in static ergodic fields have reached a high level of sophistication [1–4] and are generally accepted to require a much larger numerical effort. We will, nevertheless, investigate in the future, also to what extend these simple schemes can correctly reproduce also the transport across ergodic layers of finite extent.

Appendix A. Numerical scheme in general (multi-helicity) formulation

In the general case in periodic cylindrical geometry, we still express the magnetic field (reduced MHD formulation) as

$$\vec{B} = B_{0t}\left(\frac{r}{q(r)R}\vec{e}_\theta + \vec{e}_z\right) + \nabla\psi \times \vec{e}_z \tag{A.1}$$

but write the perturbation field as truncated Fourier series in

$$\Psi = \sum_{m,n} \Psi_{mn}(r)\mathrm{e}^{\mathrm{i}(m\theta+n\phi)} = \sum_{\vec{k}} \Psi_{\vec{k}}\mathrm{e}^{\mathrm{i}\vec{k}\cdot\vec{\xi}},$$

with integer m,n, and $\psi_{-\vec{k}} = \psi^*_{\vec{k}}$. In the following we will use the unit vectors $\vec{b} = \vec{B}/|B| \approx \vec{B}/B_{0t}$; the specification of the perturbation fields in terms of a stream function ensures the divergence-freeness of $\vec{B}$, though

not of $\vec{b}$. The formulae below would therefore also hold in the case of a more general representation of the perturbation field.

The heat sources and sinks Q and the temperatures are likewise expressed as

$$Q = \sum_{\vec{k}} Q_{\vec{k}} e^{i\vec{k}\cdot\vec{\xi}}, \quad T = \sum_{\vec{k}} T_{\vec{k}} e^{i\vec{k}\cdot\vec{\xi}}.$$

In finite differences in r and in terms of the Fourier coefficients, the heat transport equation (Eqs. (1) and (2)) reads

$$\begin{aligned}\frac{3}{2} n^i \frac{\partial T^i_{\vec{k}}}{\partial t} = &- \left(\begin{array}{l} i \dfrac{(\vec{k}\cdot\vec{b}_0)^{i+1/2} q^{i+1/2}_{\parallel,\vec{k}} + (\vec{k}\cdot\vec{b}_0)^{i-1/2} q^{i-1/2}_{\parallel,\vec{k}}}{2} \\ \\ + \frac{1}{2} \sum\limits_{\vec{k}',\vec{k}''} \delta(\vec{k} - \vec{k}' - \vec{k}'') \cdot \left(\begin{array}{l} \dfrac{r^{i+1/2} b^{i+1/2}_{\vec{k}',r} q^{i+1/2}_{\parallel,\vec{k}''} - r^{i-1/2} b^{i-1/2}_{\vec{k}',r} q^{i-1/2}_{\parallel,\vec{k}''}}{r^i \Delta r} \\ \\ + \dfrac{i\left((\vec{k}''\cdot\vec{e}_\theta)^{i+1/2} b^{i+1/2}_{\vec{k}',\theta} q^{i+1/2}_{\parallel,\vec{k}''} + (\vec{k}''\cdot\vec{e}_\theta)^{i-1/2} b^{i-1/2}_{\vec{k}',\theta} q^{i-1/2}_{\parallel,\vec{k}''} \right)}{2} \end{array} \right) \end{array} \right) \\ &+ \frac{1}{r^i (\Delta r)^2} \left(r^{i+1/2} n^{i+1/2} \chi_\perp^{i+1/2} (T^{i+1}_{\vec{k}} - T^i_{\vec{k}}) - r^{i-1/2} n^{i-1/2} \chi_\perp^{i-1/2} (T^i_{\vec{k}} - T^{i-1}_{\vec{k}}) \right) \\ &- \frac{n^{i+\frac{1}{2}} \chi_\perp^{i+\frac{1}{2}} (\vec{k}\cdot\vec{k})^{i+\frac{1}{2}} (T^{i+1}_{\vec{k}} + T^i_{\vec{k}}) + n^{i-\frac{1}{2}} \chi_\perp^{i-\frac{1}{2}} (\vec{k}\cdot\vec{k})^{i-\frac{1}{2}} (T^i_{\vec{k}} + T^{i-1}_{\vec{k}})}{2} + Q^i_{\vec{k}}, \end{aligned} \tag{A.2}$$

with

$$q^{i+1/2}_{\parallel,k} = -\sum_{k',k''} \delta(k - k' - k'') \left(n^{i+1/2} (\chi^{i+1/2}_\parallel - \chi^{i+1/2}_\perp) \right) \left(b^{i+1/2}_{k',r} \frac{T^{i+1}_{k''} - T^i_{k''}}{\Delta r} + i(k''\cdot e_\theta) b^{i+1/2}_{k',\theta} \frac{T^{i+1}_{k''} + T^i_{k''}}{2 r^{i+1/2}} \right) \Big/ 2, \tag{A.3}$$

where we have implemented the same principle for the radial discretisation as in Eqs. (13) and (15). The above system of equation requires selection of suitable subsets of vector-components $\vec{k}$ in the 2-d Fourier space and rules how to truncate the inclusion of terms in Eqs. (A.2) and (A.3). The discussion in Section 2, and the results of the test calculations shown in Fig. 12 highlight the danger of allowing for unbalanced heat flux contributions to $q_\parallel$ by including too high-order terms $T_{\vec{k}''}$. We have countered this by cutting the heat fluxes (Eq. (A.3)) at the same $\vec{k}$ as the temperatures.

References

[1] A.M. Runov, D. Reiter, S. Kosilov, in: 25th EPS Conference on Fusion and Plasma Physics, Prague 1998, Europhysics Conference Abstracts vol 22c, p. 1726.
[2] A. Runov, et al., Phys. Plasmas 8 (2001) 916;
A. Runov, et al., J. Nucl. Mater. 313–316 (2003) 1292.
[3] Y. Feng, F. Sardei, J. Kisslinger, J. Nucl. Mater. 266–269 (1999) 812.
[4] N. McTaggart, Higher order methods for conduction-convection problems with high anisotropy, PhD thesis, University Greifswald, 2003.
[5] B.D. Scott, Phys. Plasmas 8 (2000) 447.
[6] K. Lerbinger, J.F. Luciani, J. Comp. Phys. 97 (1991) 444.
[7] H. Lütjens, J.F. Luciani, Phys. Plasmas 3 (1997) 4192.
[8] R. Sovinec, et al., Phys. Plasmas 10 (2003) 1727.
[9] R. Sovinec, et al., J. Comp. Phys. 195 (2004) 355.
[10] W. Park, et al., Phys. Rev. Lett. 75 (1995) 1763.
[11] L.E. Sugiyama, W. Park, Phys. Plasmas 7 (2000) 4644.

[12] Q. Yu, S. Günter, G. Giruzzi, K. Lackner, M. Zabiego, Phys. Plasmas 7 (2000) 312.
[13] Q. Yu, S. Günter, K. Lackner, Phys. Plasmas 11 (2004) 140.
[14] R. Fitzpatrick, Phys. Plasmas 2 (1995) 825.
[15] M. Shashkov, Conservative Finite-difference Methods on General Grids, CRC Press, Boca Raton, FL, 1996.
[16] B.B. Kadomtsev, O.P. Pogutse, Sov. Phys.-JETP 38 (1974) 283.
[17] H.R. Strauss, Phys. Fluids 19 (1976) 134.